Tailoring the frictional properties of granular media

Sonia Utermann,[1] Philipp Aurin,[1] Markus Benderoth,[1] Cornelius Fischer,[2] and Matthias Schröter[1,*]
[1]*Max Planck Institute for Dynamics and Self-organization, Am Faßberg 17, D-37077 Göttingen, Germany*
[2]*Abt. Sedimentologie/Umweltgeologie, GZG, Georg-August-Universität Göttingen, Goldschmidtstraße 3, D-37077 Göttingen, Germany*
(Received 31 May 2011; revised manuscript received 4 August 2011; published 22 September 2011)

A method of modifying the roughness of soda-lime glass spheres is presented, with the purpose of tuning interparticle friction. The effect of chemical etching on the surface topography and the bulk frictional properties of grains are systematically investigated. The surface roughness of the grains is measured using white-light interferometry and characterized by the lateral and vertical roughness length scales. The underwater angle of repose is measured to characterize the bulk frictional behavior. We observe that the coefficient of friction depends on the vertical roughness length scale.

DOI: 10.1103/PhysRevE.84.031306 PACS number(s): 45.70.−n, 81.65.−b

I. INTRODUCTION

Experiments have confirmed that friction plays an important role in the physics of static granular materials. It was demonstrated that the random loose packing volume fraction decreases with increasing interparticle friction coefficient [1,2]. The role of friction on force chains was investigated in Ref. [3]. If static granular media are described by a statistical mechanics approach [4], a "configurational temperature" can be defined, which depends on friction [5].

Friction plays a vital role in granular dynamics too, for instance, in the case of granular material undergoing shear [6–8]. The effect of friction in granular materials under shear in a linear, split-bottomed shear cell filled with layers of high- and low-friction grains has been investigated [6]. Here it was shown that the position of the shear band depends on the layering of the two types of grains. It has been shown experimentally that friction can also play an important role in granular segregation [9,10], for example, in the sharp transition from the reverse Brazil-nut effect to the Brazil-nut effect [10], but other work shows that this is not always the case [11]. The dynamical properties of avalanches were shown to depend on interparticle friction, and two friction-dependent scenarios for granular avalanches on an incline were identified [12–14].

However, none of the above work was made with particles of the same material and shape but more than two coefficients of friction. In this study it is shown that it is possible to tune the topographic properties of soda-lime glass grains, making interparticle friction a control parameter for some types of beads and thus allowing the systematic quantitative study of the principles underlying granular phenomena such as those mentioned above. Figure 1 shows the surfaces of grains when they are untreated and after etching with the two protocols we describe below.

The article is structured as follows: In Sec. II the chemical etching protocols are described. The analysis of the grain roughness follows in Sec. III. In Sec. IV we present the bulk frictional properties of the grains measured by the underwater angle of repose, and in Appendix C a bulk measure of roughness is presented.

*matthias.schroeter@ds.mpg.de

II. ETCHING GLASS GRAINS

Usually hydrofluoric acid (HF) is used to etch glass [3,15]. However, HF alone is unpleasant to work with and is harmful to the environment [16]. Furthermore, our experiments with dilute HF showed highly inhomogeneous etching unconducive to our purpose, as demonstrated in Fig. 2. Ammonium bifluoride showed better etching properties (Fig. 1) as well as better handling: An aqueous solution of ammonium bifluoride will contain only small amounts of free HF, according to the set of equilibrium:

$$\begin{aligned} NH_4FHF \rightleftharpoons NH_4^+ + FHF^- \rightleftharpoons NH_4^+ + HF + F^- 3HF \\ + 2H_2O \rightleftharpoons FHF^- + F^- + 2H_3O^+. \end{aligned} \quad (1)$$

A protocol was developed using ammonium bifluoride that optimizes the flow properties of the etch solution while releasing little HF and etching as homogeneously as possible [17].

A. Roughening protocol

This is an HF etching procedure, so the utmost care must be observed during all steps in order to avoid chemical burns. Since the procedure is one to etch glass, plastic laboratory ware should used.

(1) 14 parts by mass of liquid glycerine, $C_3H_8O_3$, and six by mass of distilled water are heated in a water bath to 90°C.

(2) Six parts by mass of solid ammonium hydrogendifluoride, NH_4HF_2, and one part by mass of solid granulate iron(III)chloride-hexahydrate, $FeCl_3 \cdot 6H_2O$ (a catalyst), are added.

(3) An oversaturated solution is produced by mixing vigorously at 90°C.

(4) The solution is cooled under agitation until it is cool enough to be placed in the centrifuge.

(5) The oversaturated solution is centrifuged until the clear solution is separated from the undissolved solute (about 15 minutes).

(6) The solution is added to the glass grains and shaken vigorously. After the desired etching time has passed, the solution is poured out, and the grains thoroughly washed with distilled water.

A separate etching procedure to make the grains smoother was also employed. This method was published by Schel-

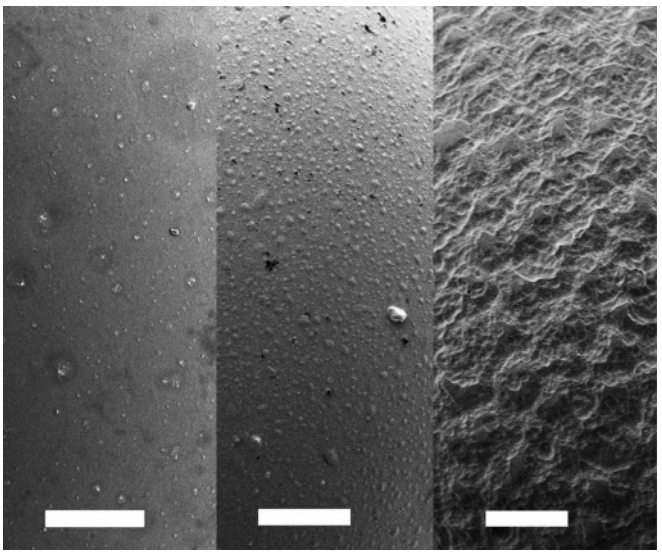

FIG. 1. Scanning electron microscope images of the surfaces of MoSci glass spheres of diameter 146 ± 19 μm (small Mo-Sci). Left: Smoothed by NaOH. Center: Untreated. Right: Etched for 4 min. The white bars are 10 μm long.

lenberger and Logan [18], To smoothen the grains, they are immersed in 12.5 M sodium hydroxide, NaOH, for 30 min, under occasional agitation.

We use soda-lime glass grains from two different manufacturers and in two different sizes. These are presented in Table I.

We perform seven treatments on each type of glass grain: smoothed for 30 min in NaOH, as supplied by the manufacturer ("unetched"), and roughened for 30 s and 1, 2, 3, and 4 min.

The effect of etching on particle size was measured using a Retsch Technology Camsizer. The particle size distribution of 200 000 grains of each batch was measured. The reduction in grain diameter after 4 min of etching with the roughening protocol is very small: between unresolvable within experimental error for the large Mo-Sci to a reduction of 3.5 ± 1.5 μm (a reduction of 2.4%) for the small Mo-Sci grains. The smoothing protocol does not bring about a resolvable reduction in diameter. The width of the size distributions also remains constant within experimental error.

TABLE I. The types of grains used in this study. The particle diameter and standard deviation (STD) was measured using a Camsizer, as outlined below.

Name	Diameter (μm)	STD (μm)	Symbol
Small Mo-Sci [19]	146	19	▲
Cataphote [20]	221	40	□
Large Mo-Sci	240	20	•

III. GRAIN ROUGHNESS

The grain surface topography was measured using white-light vertical scanning interferometry (WLI; ZeMapper, Zemetrics Inc., Tucson, AZ, USA) [21]. WLI is an optical surface scanning method that is able to provide nm height resolution over a large field of view. This enables the characterization and quantification of surface topography variations of, for example, natural grains, reacted crystal surfaces, and mineral aggregates [22]. The principle of operation is shown in Fig. 3. After passing through an external beam splitter, the white light passes through a temperature-stabilized Mirau objective (magnification: 160×). The objective is equipped with a second, internal, beam splitter. One beam is reflected by a stationary reference mirror, the other by the sample surface. The two light beams differ in optical path length as a function of the distance to the sample surface. The resulting interference pattern is captured by a high-resolution charge-coupled device (CCD). The focal plane of the interference pattern is scanned through the sample. From the collected interference pattern data, a height map is calculated. The vertical resolution of the data set is <1 nm; the maximum field of view applied in this study is 80 × 80 μm (Figs. 3 and 4).

For the WLI measurements, glass grains are bonded to glass microscope slides with ultraviolet-curable adhesive (Norland Optical Adhesive 61) and sputter coated with 40 nm gold.

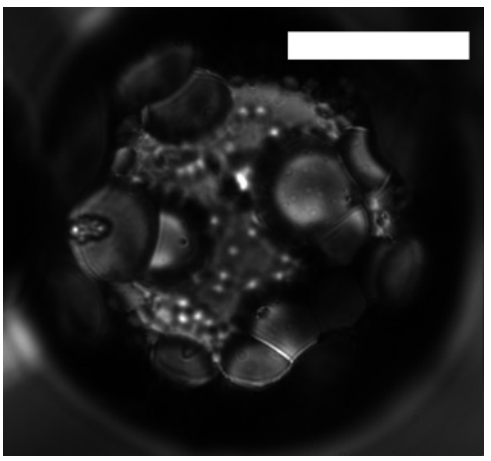

FIG. 2. Optical micrograph of a glass sphere etched in HF. The white bar is 50 μm long. Instead of homogeneous surface roughening, large craters are produced.

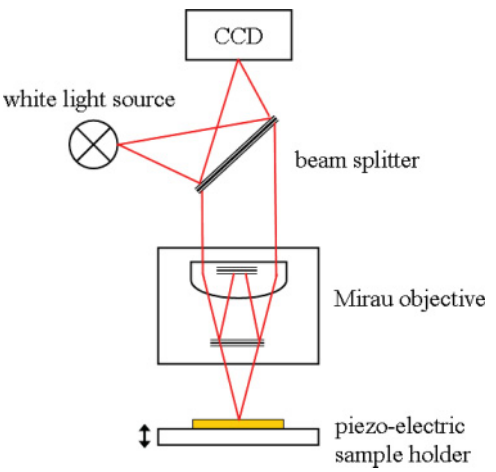

FIG. 3. (Color online) Principle of operation of a vertical scanning interferometric microscope.

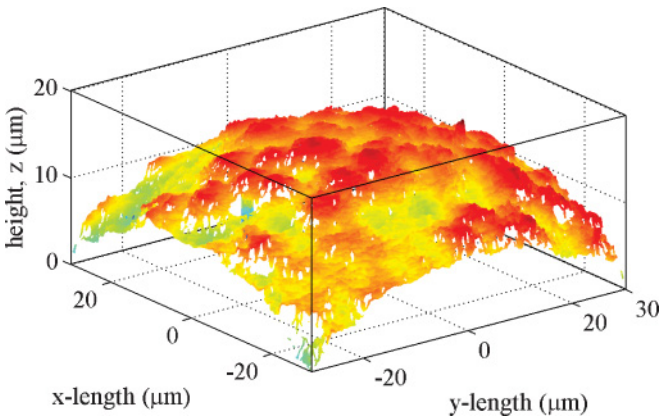

FIG. 4. (Color online) Height map of the cap of a large Mo-Sci grain etched for 4 min.

A. Roughness analysis

Characterizing roughness alone is a complex endeavor, and there is a variety of tools available to do so [23]. We use the height difference correlation function [24]. However, when measuring the roughness of spheres, one is presented with additional, unique problems. To obtain reliable statistics, a large field of view is necessary. However, the curvature of the grain means that the measurement method must have a large enough dynamic range to be able to measure nanoscale features over a height range of several μm. WLI proved to be better than AFM for this purpose.

Once a height map, $z(x,y)$, has been obtained, this may not be treated as a plane, since it is a projection of a sphere surface onto a plane, which can never be simultaneously conformal and distance conserving [26]. It is also necessary to make an angle-of-sight correction to account for having measured height in the z coordinate instead of in the radial direction. This correction is explained in Appendix A. Additionally, a batch of soda-lime glass grains will not consist only of perfectly spherical grains.

For each batch of grains, 10–15 grains are analyzed. From the surface relief measurement, the typical surface feature size characterized by a vertical ξ_{vert} and a lateral length scale ξ_{lat} is measured.

For a one-dimensional interface, ξ_{vert}, ξ_{lat}, and the Hurst exponent H are obtained from the (second-order) height difference correlation function [24]:

$$C(L) = \langle [h(x+L) - h(x)]^2 \rangle^{1/2}, \tag{2}$$

where h is the height of the interface at position x or $x+L$ (Fig. 5). For the surface of a rough sphere described in spherical polar coordinates, the height difference correlation becomes

$$\rho(L) = \langle [r'(\theta',\phi') - r(\theta,\phi)]^2 \rangle^{1/2}, \tag{3}$$

where the points $r(\theta,\phi)$ and $r'(\theta',\phi')$ are separated by the correlation distance L. On a sphere, L is the great-circle distance between the two points calculated using the spherical cosine law:

$$L = R \arccos[\cos\theta\cos\theta' + \sin\theta\sin\theta'\cos(\phi'-\phi)], \tag{4}$$

where R is the sphere radius. The angle brackets indicate an ensemble average for one L.

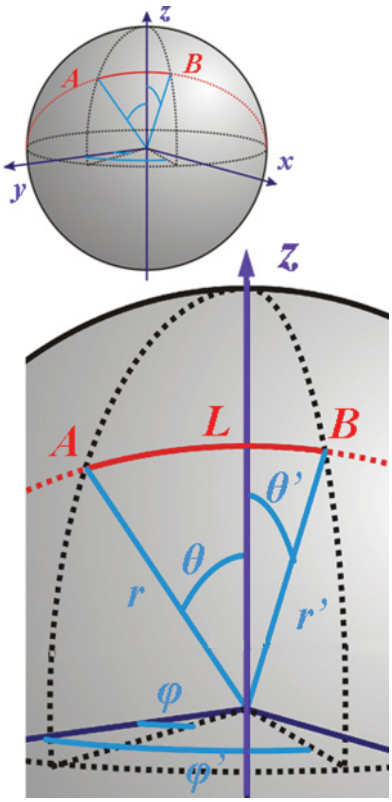

FIG. 5. (Color online) The method employed to measure roughness takes account of the spherical topology of the grain. The height difference correlation $\rho(L)$ between pairs of points $r(\theta,\phi)$ and $r'(\theta',\phi')$, separated by their great-circle distance L is calculated. R is the radius of the grain.

The height difference correlation $\rho(L)$, on a double logarithmic scale, yields the vertical and lateral saturation length scales, ξ_{vert} and ξ_{lat}, for a given etch time. This is the position at which a crossover between a power-law-type behavior and a saturation plateau occurs and is illustrated in Fig. 6.

The roughness length scales are obtained from the WLI micrographs of the spheres by the following steps: first, the WLI measurement is performed over a field of view of 80 $\times$ 80 μm (60 $\times$ 60 μm for the small Mo-Sci). The radius of the grain R is measured by optical micrography. The data is cropped to 60 $\times$ 60 μm (30 $\times$ 30 μm) to remove the bad pixels at the edges, then processed to remove spurious data adjacent to known bad pixel sites. Bad pixels make up less than 1% of the cropped data, and they are mostly at the edges where the effect of grain curvature is highest. Next, the measured R and an estimate of the x and y positions of the "north pole" are taken as start values for a hemispherical fit to the data. Using the position of the center of the grain, x_0, y_0, and z_0, obtained from the hemispherical fit, the data are converted to spherical polar coordinates r,θ, and ϕ.

Following this, $\rho(L)$ is calculated, taking account of the angle-of-sight correction (Appendix A). Three million randomly chosen pairs of points are taken to calculate $\rho(L)$ for each grain. The vertical length scale ξ_{vert} is obtained by laying spline through $\rho(L)$; the length L_{kink} at which the slope of this spline becomes zero is detected. $\rho(L)$ is averaged for $L > L_{\text{kink}}$, giving ξ_{vert}. A linear fit through the first five data

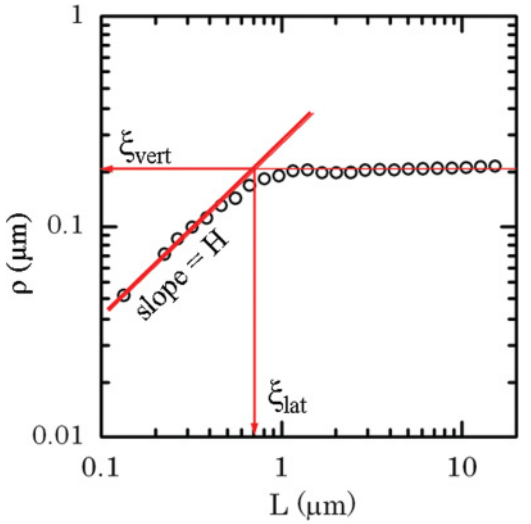

FIG. 6. (Color online) The roughness, $\rho(L)$, on a double logarithmic scale, yields the vertical and lateral saturation length scales, ξ_{vert} and ξ_{lat}, here for a Cataphote grain etched for 30 s. The slope of the fit through the first five data points is the Hurst exponent H.

points gives the Hurst exponent, H. The crossover of the linear fit and the plateau (ξ_{vert}) gives ξ_{lat}.

Strong asphericity in the grain will lead to distortion of the roughness analysis, since our analysis assumes a spherical topology. To establish the quality of the data, radial averaging is performed (see Appendix B), and data from aspherical grains are discarded. Of the 15 grains measured per batch, on average two were rejected for asphericity.

B. Roughness results

The effect of etching on the topography of glass grains is shown in Figs. 7 and 8, where the mean vertical and lateral roughness length scales, ξ_{vert} and ξ_{lat}, respectively, are plotted as a function of NH_4FHF etch time.

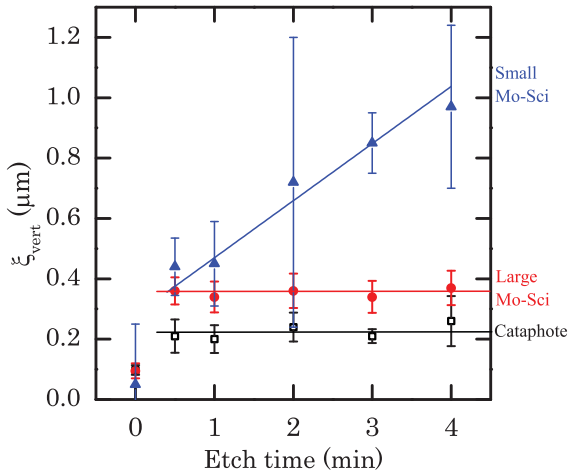

FIG. 7. (Color online) The mean vertical roughness length scale ξ_{vert} as a function of NH_4FHF etch time. In this and all subsequent plots, the error bars are the standard deviation; for each grain type 10–15 grains were measured. The linear fit through small Mo-Sci points and the means of ξ_{vert} are in the range of 30 s to 4 min.

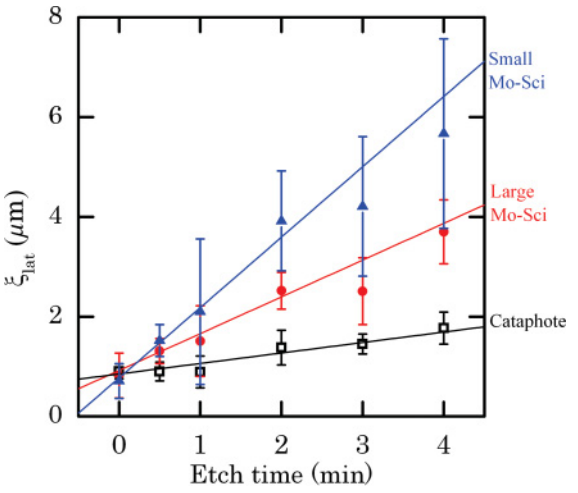

FIG. 8. (Color online) The mean lateral roughness length scale ξ_{lat} as a function of NH_4FHF etch time.

From Figs. 7 and 8, one sees that there are two types of roughening etching behavior: a monotonic increase in feature width and depth with etch time for the small Mo-Sci grains, where ξ_{vert} increases at an approximate rate of 0.17 μm per minute and ξ_{lat} at a rate of 1.4 μm per minute; and a broadening behavior for the two larger types of grains, whereby surface features become *wider* but not *deeper* as a function of etch time. It is not clear from our data if the change in etch mechanism is connected to the different radii or changes in the glass composition. The smoothed grains show no appreciable difference to the unetched grains and are omitted from the plots.

The Hurst exponent may also influence grain interactions [27]. However, as can be seen from Fig. 6, the power-law regime of $\rho(L)$ exists over less than an order of magnitude, so caution must be exercised in interpreting the behavior of the Hurst exponent H as a function of etch time (Fig. 9). We see $0 < H \leqslant 1$ for all 21 grain types. H shows a slight downward trend with increasing etch time, which is the same for all three

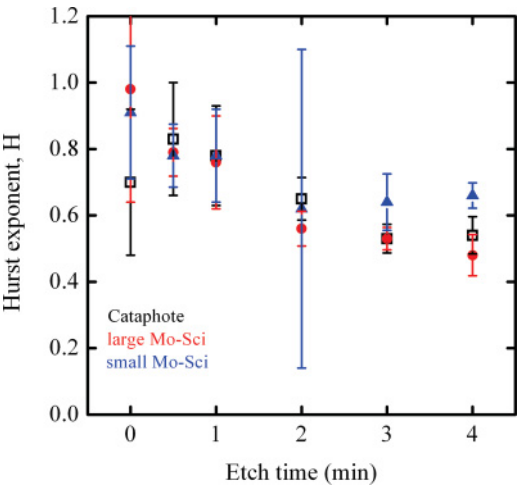

FIG. 9. (Color online) The mean Hurst exponent H as a function of NH_4FHF etch time.

grain sets, suggesting that the Hurst exponent can also be tuned by the etching protocols presented here.

It is desirable to be able to measure surface roughness in bulk samples. A possible method for doing this, using a carbonated soft drink, is demonstrated in Appendix C.

IV. BULK FRICTIONAL PROPERTIES

In this section, the angle of repose α is measured to characterize the bulk frictional behavior; to eliminate electrostatic and capillary attraction between grains, the measurements are made under water.

A. Angle-of-repose measurements

The angle of repose of each sample is measured using the setup described in Fig. 10. A cell 25 cm wide, 30 cm high, and 40 grain diameters deep is filled with water [28]. The water temperature is kept at $21 \pm 0.5^{\circ}$C for all experiments to keep the viscosity constant. An upper reservoir is filled with the granular sample. Then grains are allowed to flow to the bottom part of the cell at a rate of approximately 140 grains/s. After an avalanche has occurred, the flow of grains to the pile is stopped. The pile is photographed with a black-and-white CCD with 1 megapixel and 8-bit depth. Each photograph is binarized using a threshold that is chosen automatically to fall between the peaks of its bimodal gray-level histogram. The top and bottom edges of the pile are detected, and the location of the linear part of the pile is detected by laying a spline through the line describing the top of the pile. Within this range, linear fits are made to the top and bottom of the pile; the angle between them is the angle of repose α. The measurement was repeated 10–20 times per grain type. The resolution in α is $\pm 0.15^{\circ}$

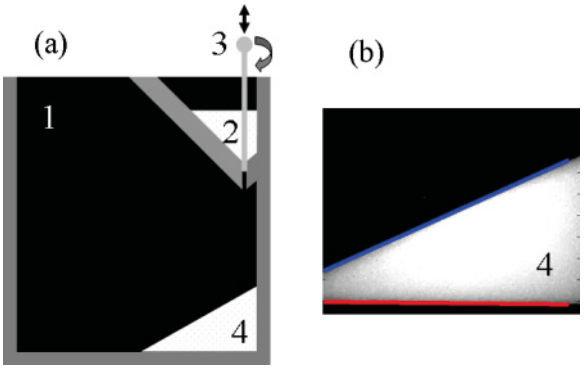

FIG. 10. (Color online) Angle of repose measurement method. (a) A sketch of the setup: A cell [1] 25 cm wide, 30 cm high, and 40 grain diameters deep is filled with water. The reservoir [2] is filled with the granular sample. The funnel rod [3] is raised by a screw thread to open the hole enough to let grains flow to the bottom part of the cell [4]. After an avalanche has occurred, the rod is lowered enough to induce granular arching, thus stopping the flow of grains. (b) CCD image of the pile. Linear fits to the bottom and top edges of the pile give the angle of repose (see text).

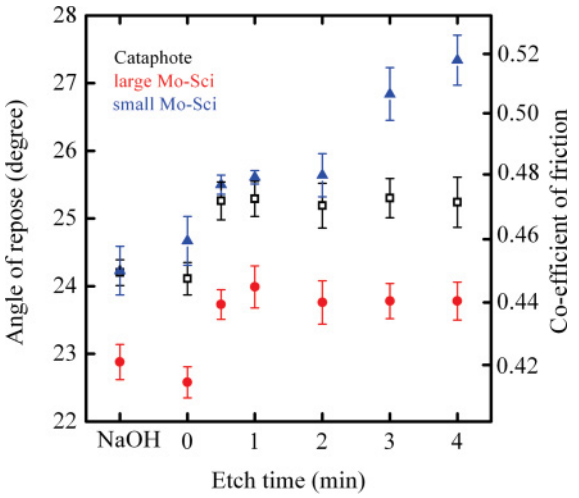

FIG. 11. (Color online) Underwater angle of repose as a function of roughening etch time. The smoothing protocol, NaOH, is plotted on the negative x axis. The error bars are the standard deviation. The coefficient of friction is computed by $\mu = \tan\alpha$, where α is the angle of repose [33].

B. Results

Figure 11 shows α as a function of roughening etch time. For the small Mo-Sci grains, the angle of repose increases monotonically from about 24° to over 27° as a function of etch time. As in the roughness measurements, the smoothed grains do not show an appreciable difference from the unetched grains.

The Cataphote and large Mo-Sci grains again show different behavior from the small grains. Again, their behavior is a step function: Unetched and smoothed grains have an angle of repose about 1° less than grains etched in NH_4FHF for 30 s or longer. The appearance of these trends is similar to ξ_{vert} as a function of etch time shown in Fig. 7. However, the Cataphote grains, whose ξ_{vert} is always lower than the large Mo-Sci grains, have a consistently *larger* angle of repose.

One reason for this discrepancy could be the different fractions of nonspherical grains present in the Cataphote and Mo-Sci samples. The average length-to-width ratio, l/b_{ave}, of the unetched Cataphote and large Mo-Sci grains was measured using a Retsch Technology Camsizer (sample size of 7000 grains). With $l/b_{ave} = 1.17$, the Cataphote grains show a slightly greater average asphericity than the large Mo-Sci grains, $l/b_{ave} = 1.12$. It has been demonstrated that higher asphericity leads to a larger angle of repose [14]. Another reason for the discrepancy could be that the two larger types of grain also produce different packing densities ϕ, which would be a natural consequence of their asphericity [32]. Though we did not measure ϕ in this setup, we show that ϕ has a strong influence on the angle of repose (Appendix D). Again, for the larger grains, the smoothing protocol has no apparent influence on α.

A valuable result of this work is to show how the frictional properties of grains depend on their (tailored) roughness. This is illustrated in Fig. 12: The angle of repose has a dependency on ξ_{vert}, albeit a weak/noisy one. The angle of repose showed no appreciable correlation with ξ_{lat}, again suggesting that it is the *depth* of surface features, not their width, that controls the

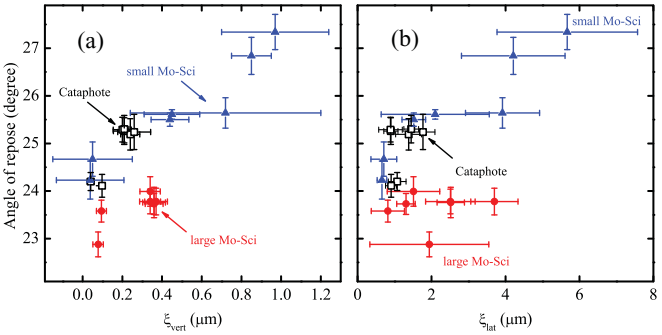

FIG. 12. (Color online) Angle of repose α as a function of correlation length scales (a) ξ_{vert} and (b) ξ_{lat}.

friction between grains. However, there is not a simple, linear dependency.

V. CONCLUSION

In this study, a method of modifying the topographical properties of soda-lime glass grains was presented, with the purpose of tuning interparticle friction. We presented a roughening and a smoothing chemical etching procedure. The surface roughness of the grains was measured using white-light interferometry and characterized using the height difference correlation function. Two types of roughening etching behavior were observed: a monotonic increase in feature width and depth with etch time for the small grains, and a broadening behavior for the two larger types of grains, whereby surface features became wider but not deeper as a function of etch time. We concluded that, when changing the roughness of glass grains, the type of grain matters. With the three types of grains we used, we are unable to distinguish whether this is due to size or material composition. The smoothing protocol made little difference to the surface roughness. The underwater angle of repose α was measured to characterize the bulk frictional behavior. For the small grains, α increased monotonically as a function of etch time. The two larger types of grains showed a different behavior: Unetched and smoothed grains had an angle of repose about 1°less than etched grains. In the appendices, we present a suggestion for measuring grain roughness in bulk samples.

The ammonium bifluoride etching technique presented here allows the experimentalist to modify the roughness of glass spheres. Grains with tunable roughness are the ideal work-horse for experimental studies of wet (or "humid") granular systems [27] or of hydrodynamic interactions between grains in viscous fluids [34,35]. It is shown that changing the surface roughness of grains directly changes the way they behave in the bulk. In addition, the systems already shown experimentally to depend on friction, which were reviewed in Sec. I; this has other important consequences for granular community in that it paves the way for comparison with simulations, where friction between grains is a typical control parameter. Additionally, the ability to tailor glass grains will allow systematic study of the role of friction in the static and dynamic behavior of granular material, for instance, granular segregation and pattern formation, avalanching, and (shear)flow, packing, and force chains.

ACKNOWLEDGMENTS

We extend our thanks to Karina Sand of the University of Copenhagen for the scanning electron micrographs; to Sabine Schlüsselburg of the University of Magdeburg for the use of the Camsizer; to Harald Heinrici of Schwedes und Schulze Schüttguttechnik, Tamas Börzsönyi of the Research Institute for Solid State Physics and Optics in Budapest, and Julie Murison and Udo Schminke of the Max Planck Institute for Dynamics and Self-organization for enlightening discussions; and to Steve Clappison for the Mentos and Diet Coke idea.

APPENDIX A: ANGLE-OF-SIGHT CORRECTIONS

When analyzing the roughness of the glass spheres, we make an angle-of-sight correction to account for our having measured height in the z coordinate instead of in the radial direction. This is shown in Fig. 13. We correct the vertical height, $\Delta z(x,y)$, to a radial feature size, $\Delta r(\theta,\phi)$, by

$$\Delta r = \frac{\Delta z}{\cos\theta}. \tag{A1}$$

The relevance of this correction can be estimated for the worst-case scenario: a feature at the outermost corner of the region of interest on a small Mo-Sci grain. In this case, $\theta = 37°$; thus omitting this correction results in an error of 26%.

APPENDIX B: RADIAL AVERAGING TO TEST FOR ASPHERICAL GRAINS

Strong asphericity in the grain will lead to distortion of the roughness analysis, since our analysis assumes a spherical topology. In our case, this is particularly true of the two smoothest sets of grains. To check if the grain is

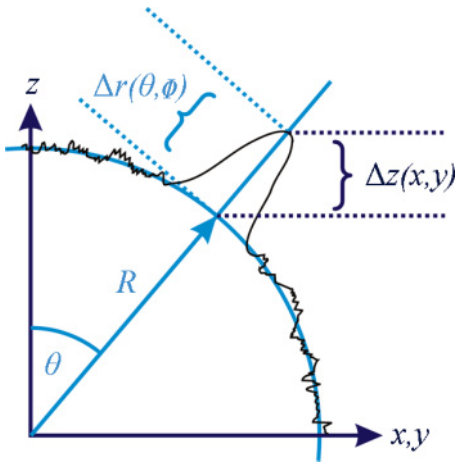

FIG. 13. (Color online) When analyzing the roughness of the glass spheres, we need to make an angle-of-sight correction to account for our having measured height in the z coordinate instead of in the radial direction. R is the sphere radius, and $\Delta z(x,y) = h(\theta,\phi)$ is the height of the grain profile measured vertically from above. The correct radial height of the feature is given by $\Delta r = \frac{\Delta z}{\cos\theta}$.

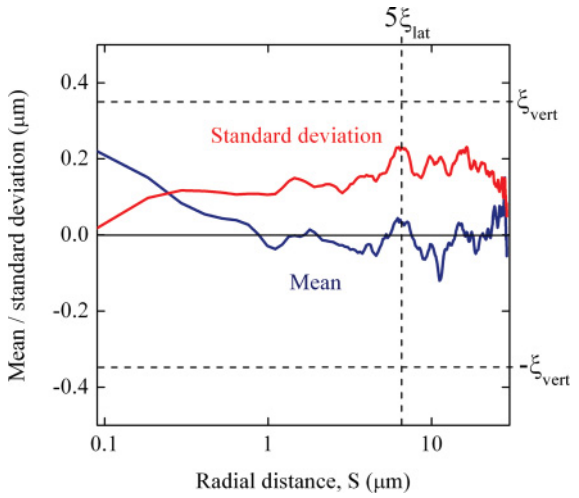

FIG. 14. (Color online) Radial average and standard deviation of a large Mo-Sci grain etched for one minute. This grain is accepted: both lines remain within the range $[-\xi_{vert}...\xi_{vert}]$ for $L < 5\xi_{lat}$.

spherical enough that the roughness data are not falsified, radial averaging of the relief measurement of the grain is performed:

$$\langle \Delta r(\theta) \rangle|_{all\phi}. \tag{B1}$$

For a perfect sphere, both the radial mean and the standard deviation are zero for all θ. For rough grains, small deviations from zero are expected, for aspherical grains large deviations. Since our analysis depends on our ability to locate the kink in $\rho(L)$, it is vital that the mean and the standard deviation are smaller than the length scales we wish to measure, ξ_{vert} and ξ_{lat}. We set the criterion that, if the radial mean OR standard deviation is greater than ξ_{vert} for any angle corresponding to a radial distance $S < 5\xi_{lat}$, we reject the grain from our analysis, on the grounds that its asphericity has an influence on its $\rho(L)$ at the relevant length scales. This is illustrated in Figs. 14 and 15.

Of the 15 grains measured per batch, on average two were rejected for asphericity.

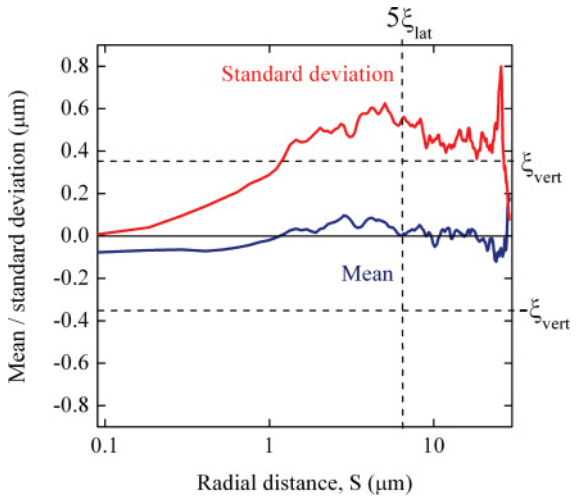

FIG. 15. (Color online) Radial average and standard deviation of a different large Mo-Sci grain etched for 1 min. This grain is rejected: the standard deviation exceeds the range $[-\xi_{vert}...\xi_{vert}]$ for $L < 5\xi_{lat}$.

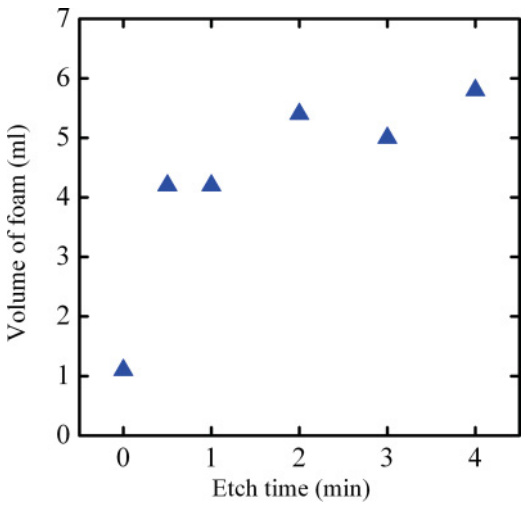

FIG. 16. (Color online) Maximum volume of cola foam as a function of etch time (small Mo-Sci).

APPENDIX C: USING A CARBONATED SOFT DRINK TO MEASURE THE ROUGHNESS OF GRAINS

The popular experiment in which a geyser is produced by dropping Mentos into a bottle of Diet Coke [36] was studied systematically by T. S. Coffey [37]. She concluded that the surface roughness of the sweets is one of the main causes of the reaction, namely, surface features provide nucleation sites for bubbles of carbon dioxide. We use this principle in a prototype experiment for measuring surface roughness in bulk granular samples using a carbonated soft drink.

The experimental method is as follows: 4 ± 0.05 ml of a freshly opened carbonated soft drink (Coca-Cola) is poured into a measuring cylinder. Pouring is smooth to minimize premature nucleation of bubbles. Here 500 ± 0.5 mg of granular sample (small Mo-Sci) is added through a funnel. The maximum volume of cola, beads, and foam is measured, and the volume of the grains and the initial volume of cola subtracted.

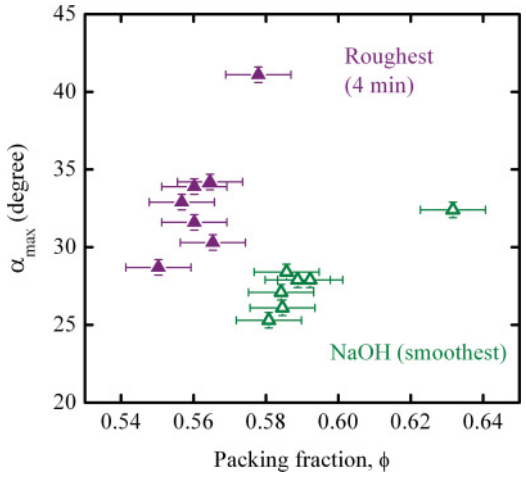

FIG. 17. (Color online) Angle of maximum stability α_{max} as a function of packing fraction for two types of grains: small Mo-Sci etched for 4 min (purple closed symbols) and smoothed in NaOH (green open symbols).

Figure 16 shows that there is a trend: The cola produces more foam when it comes into contact with the more strongly etched particles. Of course, not just surface roughness but also other effects, such as surface activity, buoyancy, and occupation density of nucleation sites, play a vital role in the reaction [37]. It is interesting to speculate how this method could be calibrated.

APPENDIX D: ANGLE OF MAXIMUM STABILITY AS A FUNCTION OF PACKING FRACTION

The angle of repose (pile slope after an avalanche, α) is dependent not only on the friction between grains but also on their packing density. The same is true of the angle of maximum stability (pile slope just before an avalanche, $\alpha_{\max}$), which proved to be the more accessible quantity in investigating this dependence.

The density of the grain material is determined to within 0.45 μg/cm^3 with a Micromeritics gas pyknometer. The grains are added to a cell of square cross section 4 $\times$ 4 cm, which is filled with water. A packing of grains is (re)produced on a Ling Dynamic Systems V409 shaker. The packing fraction is determined to within an error of $\pm 9 \times 10^{-3}$ by measuring the height of the packing in the container. The container is transferred to a board that is hinged at one end and raised slowly at the other, under computer control, by a stepper motor. A black-and-white CCD with 1 megapixel and 8-bit depth is used to record the surface of the granular sample while the angle of the container is increased. The camera and an LED light source are mounted such that they do not move relative to the container, thus avoiding spurious results from shadows; the camera is triggered as the stepper motor starts. Image processing is used to determine $\alpha_{\max}$ with an accuracy of $\pm 0.5^\circ$ as follows: First, subsequent images of the surface of the sample are subtracted. The subtracted images are binarized; the threshold for binarization is taken as the mean gray value for a nonmoving bed plus four standard deviations. Then, connected moving pixels are detected. A continuous moving area of more than one grain (more than 50 pixels with our optics and setup) is our definition of an avalanche. The angle at which this occurs is the angle of maximum stability $\alpha_{\max}$.

The smoothest and the roughest samples of the small Mo-Sci grains were tested. In both cases, a clear dependency of $\alpha_{\max}$ on the packing fraction ϕ was observed. The effect was strongest for the roughest grains: Here the angle increased from 29° to 41° in the range $0.55 < \phi < 0.58$.

A systematic study of the underwater flow of frictional grains as a function of initial packing fraction was made by Pailha *et al.* [38]. For fixed inclination angles, they observed that avalanching occurs more readily for lower packing fractions, a result with which our Fig. 17 is consistent.

[1] M. Jerkins, M. Schröter, H. L. Swinney, T. J. Senden, M. Saadatfar, and T. Aste, Phys. Rev. Lett. **101**, 018301 (2008).

[2] G. R. Farrell, K. M. Martini, and N. Menon, Soft Matter **6**, 2925 (2010).

[3] D. L. Blair, N. W. Mueggenburg, A. H. Marshall, H. M. Jaeger, and S. R. Nagel, Phys. Rev. E **63**, 041304 (2001).

[4] S. F. Edwards and R. B. S. Oakeshott, Phys. A **157**, 1080 (1989).

[5] M. Schröter, D. I. Goldman, and H. L. Swinney, Phys. Rev. E **71**, 030301(R) (2005).

[6] T. Börzsönyi, T. Unger, and B. Szabó, Phys. Rev. E **80**, 060302(R) (2009).

[7] K. Mair, K. M. Frye, and C. Marone, J. Geophys. Res. **107**, 2219 (2002).

[8] J. L. Anthony and C. Marone, J. Geophys. Res. **110**, B0849 (2005).

[9] G. Plantard, H. Saadaoui, P. Snabre, and B. Pouligny, Europhys. Lett. **75**, 335 (2006).

[10] S. Ulrich, M. Schröter, and H. L. Swinney, Phys. Rev. E **76**, 042301 (2007).

[11] N. A. Pohlman, B. L. Severson, J. M. Ottino, and R. M. Lueptow, Phys. Rev. E **73**, 031304 (2006).

[12] T. Börzsönyi, T. C. Halsey, and R. E. Ecke, Phys. Rev. Lett. **94**, 208001 (2005).

[13] T. Börzsönyi and R. E. Ecke, Phys. Rev. E **76**, 031301 (2007).

[14] T. Börzsönyi, T. C. Halsey, and R. E. Ecke, Phys. Rev. E **78**, 011306 (2008).

[15] G. A. C. M. Spierings, J. Mater. Sci. **28**, 6261 (1993).

[16] See material safety data sheet C. A. S. No. 7664-39-3.

[17] An alternative etch solution is described in S. H. Gimm, J. H. Kim, and T. H. Kim, US Patent 5281350 (1994), but its high viscosity does not suit it to the etching of glass grains.

[18] K. Schellenberger and B. E. Logan, Environ. Sci. Technol. **36**, 184 (2002).

[19] Manufactured by Mo-Sci Specialty Products, 4040 HyPoint North, Rolla, MO 65401, USA.

[20] Manufactured by Ferro Corp. Div. Cataphote, 1001 Underwood Drive, Jackson, MS 39208, USA.

[21] Instrument described in detail in G. K. Darbha, T. Schäfer, F. Heberling, A. Lüttge, and C. Fischer, Langmuir **26**, 4743 (2010).

[22] C. Fischer and A. Lüttge, Am. J. Sci. **307**, 955 (2007).

[23] For example, RMS roughness, (multi-)affine box-counting, power spectral analysis or wavelet analysis. The latter three are mostly used for fractal analysis. An overview of these methods can be obtained from Refs. [24] and [25].

[24] P. Meakin, *Fractals, Scaling and Growth Far from Equilibrium* (Cambridge University Press, Cambridge, 1998).

[25] I. Rodríguez Iturbe and A. Rinaldo, *Fractal River Basins* (Cambridge University Press, Cambridge, 1997).

[26] I. N. Bronstein, K. A. Semendjajev, G. Musiol, and H. Mühlig, *Taschenbuch der Mathematik*, 5th ed. (Harri Deutsch, Frankfurt am Main, 2001).

[27] T. C. Halsey and A. J. Levine, Phys. Rev. Lett. **80**, 14 (1998).

[28] For spherical particles with a fairly low friction coefficient, the influence of the side walls can be calculated [29,30] and measured experimentally [29,31]. For smooth glass beads and smooth side walls, the characteristic length of the wall effects is $B_m \approx 0.7d$, where d is the particle diameter.

[29] S. Courrech du Pont, P. Gondret, B. Perrin, and M. Rabaud, Europhys. Lett. **61**, 492 (2003).
[30] G. D. R. MiDi, Eur. Phys. J. E Soft Matter **14**, 341 (2004), and references therein.
[31] P. Jop, Y. Forterre, and O. Pouliquen, Nature (London) **441**, 04801 (2006).
[32] A. Donev, R. Connelly, F. H. Stillinger, and S. Torquato, Phys. Rev. E **75**, 051304 (2007).
[33] C. A. Coulomb, Mem. Acad. Roy. Pres. Div. Sav. **7**, 343 (1776).
[34] J. T. Jenkins and M. A. Koenders, Granular Matter **7**, 13 (2005).
[35] R. Beetstra, M. A. van der Hoef, and J. A. M. Kuipers, AIChE J. **53**, 2 (2007).
[36] Adam Savage and Jamie Hyneman, Episode 57: Mentos and Soda, Mythbusters, Discovery Channel, first aired 9th August 2006, [http://dsc.discovery.com/videos/mythbusters-diet-coke-and-mentos.html].
[37] T. S. Coffey, Am. J. Phys. **76**, 6 (2008).
[38] M. Pailha, M. Nicolas, and O. Pouliquen, Phys. Fluids **20**, 111701 (2008).